Journal of Inorganic Biochemistry 245 (2023) 112243

Contents lists available at ScienceDirect

Journal of Inorganic Biochemistry

journal homepage: www.elsevier.com/locate/jinorgbio

The role of the distal cavity in carbon monoxide stabilization in the coproheme decarboxylase enzyme from *C. diphtheriae*

Federico Sebastiani [a,1], Andrea Dali [a,1], Diego Javier Alonso de Armiño [b], Lorenzo Campagni [a], Gaurav Patil [c], Maurizio Becucci [a,***], Stefan Hofbauer [c,***], Dario A. Estrin [b,d,**], Giulietta Smulevich [a,e,*]

[a] *Dipartimento di Chimica "Ugo Schiff" DICUS, Università di Firenze, Via della Lastruccia 3-13, Sesto Fiorentino (FI) I-50019, Italy*
[b] *CONICET-Universidad de Buenos Aires, Instituto de Química Física de los Materiales, Medio Ambiente y Energía (INQUIMAE), Buenos Aires, Argentina*
[c] *University of Natural Resources and Life Sciences, Department of Chemistry, Institute of Biochemistry, Muthgasse 18, Vienna A-1190, Austria*
[d] *Universidad de Buenos Aires, Departamento de Quimica Inorgánica, Analítica y Química Física, Facultad de Ciencias Exactas y Naturales, Buenos Aires C1428EGA, Argentina*
[e] *INSTM Research Unit of Firenze, via della Lastruccia 3, Sesto Fiorentino I-50019, Italy*

ARTICLE INFO

Keywords:
Resonance Raman
Molecular dynamics simulations
Ligand binding
Coproporphyrin-dependent
Heme biosynthesis
Pathogen bacteria

ABSTRACT

This work focuses on the carbon monoxide adducts of the wild-type and selected variants of the coproheme decarboxylase from actinobacterial *Corynebacterium diphtheriae* complexed with coproheme, monovinyl monopropionyl deuteroheme (MMD), and heme *b*. The UV − vis and resonance Raman spectroscopies together with the molecular dynamics simulations clearly show that the wild-type coproheme-CO adduct is characterized by two CO conformers, one hydrogen-bonded to the distal H118 residue and the other showing a weak polar interaction with the distal cavity. Instead, upon conversion to heme *b*, i.e. after decarboxylation of propionates 2 and 4 and rotation by 90° of the porphyrin ring inside the cavity, CO probes a less polar environment. In the absence of the H118 residue, both coproheme and heme *b* complexes form only the non-H-bonded CO species. The unrotated MMD-CO adduct as observed in the H118F variant, confirms that decarboxylation of propionate 2 only, does not affect the heme cavity. The rupture of both the H-bonds involving propionates 2 and 4 destabilizes the porphyrin inside the cavity with the subsequent formation of a CO adduct in an open conformation. In addition, in this work we present data on CO binding to reversed heme *b,* obtained by hemin reconstitution of the H118A variant, and to heme *d*, obtained by addition of an excess of hydrogen peroxide. The results will be discussed and compared with those reported for the representatives of the firmicute clade.

1. Introduction

During infection, pathogens must synthesize heme or acquire it from the host to survive and thus spread the disease. Heme is typically sequestered in high-affinity heme-proteins of the host; therefore, the heme biosynthesis is a more efficient strategy for bacterial pathogens [1–3]. Coproheme decarboxylase enzymes (ChdCs) catalyze the final step within the coproporphyrin-dependent heme *b* biosynthetic

Abbreviations: ChdC, coproheme decarboxylase; *Cd*, *Corynebacterium diphtheriae*; *Cd*ChdC, ChdC from *Corynebacterium diphtheriae*; *Gs*, *Geobacillus stearothermophilus*; *Lm*, *Listeria monocytogenes*; *Sa*, *Staphylococcus aureus*; H-bond, hydrogen bond; MDS, Molecular Dynamics Simulation; MMD, monovinyl monopropionyl deuteroheme (or harderoheme); 6c, hexacoordinated; LS, low-spin; RR, resonance Raman; p_2, p_4, p_6 and p_7, propionate groups at positions 2, 4, 6 and 7; v_2 and v_4, vinyl groups at positions 2 and 4; Cld, chlorite dismutase; eqs, equivalents; WT, wild-type; Mb, myoglobin..

* Correspondence to: Giulietta Smulevich, Dipartimento di Chimica "Ugo Schiff" DICUS, Università di Firenze, Via della Lastruccia 3-13, Sesto Fiorentino (FI) I-50019, Italy.

** Correspondence to: Dario A. Estrin, CONICET-Universidad de Buenos Aires, Instituto de Química Física de los Materiales, Medio Ambiente y Energía (INQUIMAE), Buenos Aires, Argentina.

*** Corresponding authors.

E-mail addresses: maurizio.becucci@unifi.it (M. Becucci), stefan.hofbauer@boku.ac.at (S. Hofbauer), dario@qi.fcen.uba.ar (D.A. Estrin), giulietta.smulevich@unifi.it (G. Smulevich).

[1] These authors have equally contributed

https://doi.org/10.1016/j.jinorgbio.2023.112243
Received 3 March 2023; Received in revised form 28 April 2023; Accepted 1 May 2023
Available online 3 May 2023

pathway, which is mainly, but not exclusively, used by monoderm bacteria [4–7].

ChdCs accumulate heme *b* by the oxidative decarboxylation of propionate groups at positions 2 and 4 (p_2 and p_4) of coproheme to vinyls (v_2 and v_4) via two exogenous hydrogen peroxide (H_2O_2) molecules. The reaction involves first the cleavage of p_2, i.e. the formation of a monovinyl monopropionyl deuteroheme (MMD, also known as harderoheme) reaction intermediate, which undergoes a 90° rotation. This reorientation allows p_4 to get close to the catalytic residue and thus to be decarboxylated to v_4, and eventually, heme *b* is formed [8–13]. A schematic representation of the catalytic cycle of one propionate decarboxylation reaction in actinobacterial *Cd*ChdC is shown in Fig. 1.

From experimental and computational mechanistic studies on the representatives from Firmicutes (e.g. *Listeria monocytogenes* (*Lm*) [14], *Staphylococcus aureus* (*Sa*) [15] and *Geobacillus stearothermophilus* (*Gs*) [16]) and on actinobacterial *Corynebacterium diphtheriae* (*Cd*) [13,17] it was concluded that the transiently-formed MMD reaction intermediate rotates within the active site and not via a release and rebinding mechanism. For the ChdC from *Corynebacterium diphtheriae* (*Cd*ChdC), a combined spectroscopic and biochemical approach has been proved to be particularly effective in the characterization of the enzyme complexed with the coproheme, MMD and heme *b* in both the ferric and ferrous forms, during the catalytic reaction, and in the identification of the role of fundamental residues in the active site [13,17,18].

In ChdCs from Actinobacteria, unlike in Firmicutes, a distal histidine, located on a flexible loop connecting two ferredoxin-like domains, was identified as relevant for the enzymatic activity in addition to a catalytic Tyr (Y135 in *Cd*ChdC), which is completely conserved in all bacterial ChdCs [10,11]. This distal residue (H118 in *Cd*ChdC) acts as a distal base for deprotonation and subsequent heterolytic cleavage of hydrogen peroxide [10], leading to a significantly higher reactivity of *Cd*ChdC toward H_2O_2 [11,19]. Moreover, in the presence of H118 residue, a stoichiometric excess of hydrogen peroxide leads to the formation of iron chlorin-type heme *d* species [20–22]. Heme *d* formation was correlated with a potential protection mechanism from oxidative damage [23].

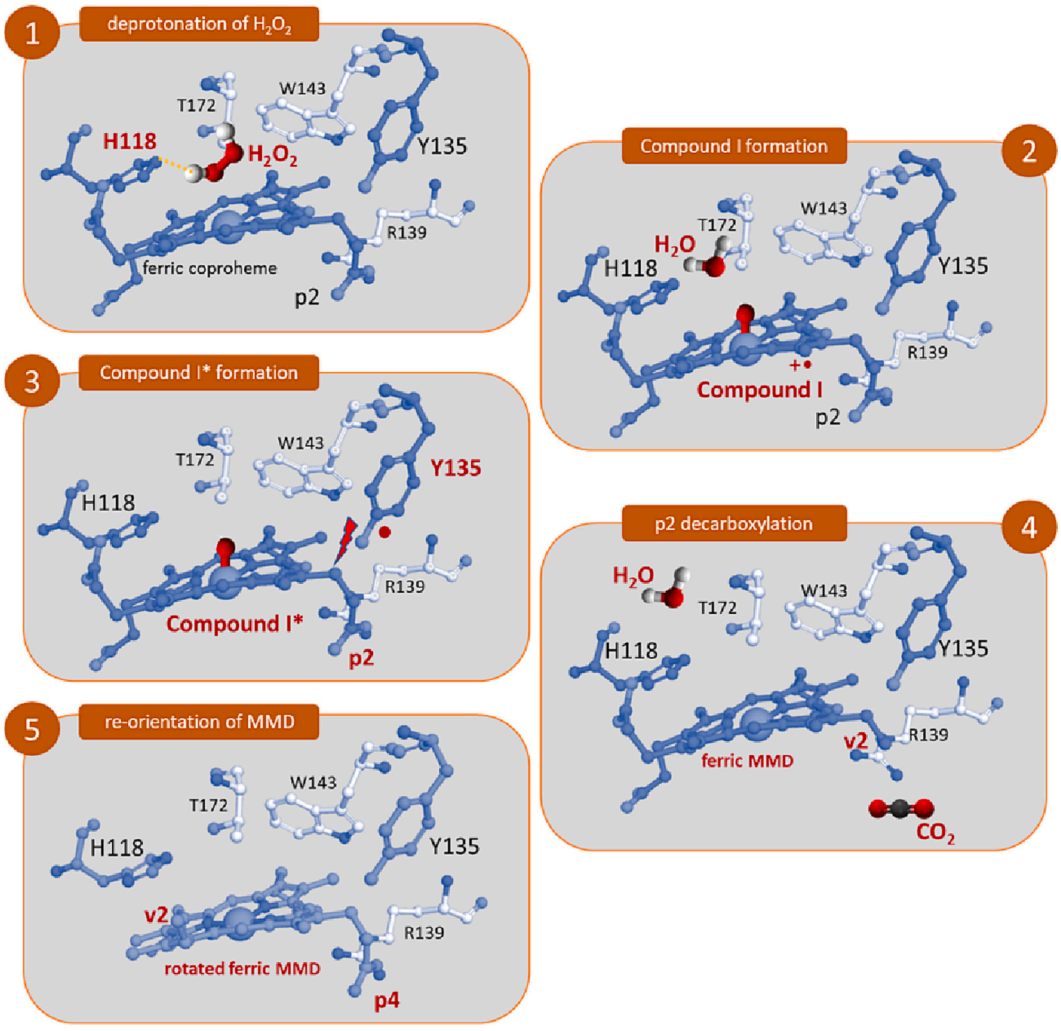

Fig. 1. Schematic representation of the catalytic cycle of one propionate decarboxylation reaction in actinobacterial *Cd*ChdC. The reaction is initiated by hydrogen peroxide approaching the ferric coproheme active site. (1) Histidine 118 acts as a distal base and is responsible for the heterolytic cleavage of H_2O_2 (orange dashed line representing the deprotonation step). (2) The ferric resting state of coproheme *Cd*ChdC is oxidized by activated (i.e. deprotonated) hydrogen peroxide to Compound I (oxoiron(IV) porphyryl radical) and water. (3) Compound I is immediately converted to Compound I* (oxoiron(IV) Y135$^{\bullet}$) by internal electron transfer. (4) The neutral tyrosine radical performs a nucleophilic attack on the β-carbon of propionate at position 2 (p2), thereby initiating its decarboxylation and formation of vinyl (v2). (5) The resulting monovinyl monopropionate deuteroheme (MMD) undergoes a rotation of approximately 90°, thereby moving p4 in the position close to Y135. The second decarboxylation reaction (of p4) was proposed to work analogously to the first decarboxylation resulting in the formation of vinyl (v4). Finally, heme *b* is released and delivered to proteins. This scheme was created based on the X-ray crystal structure of coproheme-*Cd*ChdC (PDB ID: 6XUC) [10] and MMD-*Cd*ChdC. The images during turnover are artwork for visualization purposes and not experimentally determined.

Actinobacterial ChdCs are also characterized by an arginine (R139 in *Cd*ChdC) instead of a catalytically important lysine (K151 in *Lm*ChdC and K149 in *Sa*ChdC), which is otherwise conserved in all the other clades [19]. R139 is involved in the extensive hydrogen bond (H-bond) network between the protein moiety and the propionate groups of the porphyrin, which stabilizes the substrate or the product within the active site both in the crystal [10] and in solution [18]. This arginine, bridging p_2 and p_4, has also been shown to be the most important residue for reactivity toward H_2O_2 in *Cd*ChdC [18].

Furthermore, the proximal side of ChdCs has been found to be less relevant than the distal side, since the proximal histidine does not have any H-bond interaction with the cavity residues [24,25]. Therefore, the proximal coordination is weak with respect to other structurally related enzymes (e.g. chlorite dismutases, Clds), as also shown by Fe-Im bond strength. In fact, in the ferrous heme *b* of ChdCs the wavenumber of the Fe-Im stretching mode was found between 210 (in *Cd*ChdC [17]) and 214–216 cm^{-1} (in *Lm*ChdC [26] and *Sa*ChdC [27], respectively), while in the heme *b*-Clds, it ranges from 222 cm^{-1} [28], 226 cm^{-1} [24], to 229 cm^{-1} [29].

Carbon monoxide (CO) has been extensively used both as a model exogenous ligand and as a probe sensitive to the nature and the architecture of the heme binding pocket in proteins. In fact, a positively charged electrostatic field or an H-bond between CO and a distal residue favors back-donation from the Fe dπ to the CO π* orbitals, strengthening the Fe − C bond and correspondingly weakening the C − O bond, thereby increasing the $\nu_{(FeC)}$ stretching wavenumbers and decreasing the $\nu_{(CO)}$ stretching wavenumbers. Conversely, a negative charged electrostatic field has the opposite effect. Variations in the donor strength of the trans-ligand affect the vibrational modes of carbon monoxide as well [30,31].

In this work, we investigated the role of key residues of the protein cavity of actinobacterial *Cd*ChdC in the stabilization of the incoming exogenous ligands by studying the CO adducts of the wild-type (WT) protein and selected variants in complex with coproheme, MMD and heme *b* using resonance Raman (RR) spectroscopy and Molecular Dynamics Simulation (MDS). In particular, we focused on the contributions of the distal H118 and of the amino acids of the protein moiety involved in hydrogen bonds with the propionate groups of the porphyrin during the catalytic reaction, as evolving from the coproheme substrate to the MMD reaction intermediate and finally to the heme *b* product (and heme *d* side-products). A comparative analysis of exogeneous ligand binding with data on representatives from ChdCs of the firmicute clade in terms of conserved residues was also carried out.

2. Material and methods

2.1. Generation, expression and purification of CdChdC and variants

Site-directed mutagenesis, apoprotein expression and purification of *Cd*ChdC WT protein and variants have been described previously [10,13,17,32]. Site-directed mutagenesis was performed using the QuikChangeLightning (Agilent Technologies) kit. Primers used to generate variants are reported in Ref [18]. For the variants, *Cd*ChdC WT plasmid was used as the template.

2.2. Sample preparation

Ferric coproheme powder was purchased from Frontier Scientific Inc. (Logan, Utah, USA) and dissolved in 0.5 M NaOH. All the *Cd*ChdC coproheme complexes were prepared by adding the coproheme solution to the apoprotein *Cd*ChdC diluted in 50 mM phosphate buffer, pH 7.0, with a 2:1 apoprotein:coproheme ratio. The ferric *Cd*ChdC heme *b* complexes were obtained by adding small aliquots of a 1 mM H_2O_2 stock solution to the corresponding *Cd*ChdC coproheme complexes, as detailed in Ref. [13]. The complete heme *b* formation was followed by recording the electronic absorption spectra of the variants upon addition of 2 equivalents (eqs) of H_2O_2. For the wild-type protein, the heme *b* complex was also obtained by hemin reconstitution, as already described in Ref. [17], to avoid the presence of additional iron chlorin-type heme *d* [23], or residual MMD species. For the H118A variant the heme *b* complex was prepared both by H_2O_2 titration (heme *b*) and hemin reconstitution (reversed) [17]. WT heme *d* - and Y135A coproheme *d* -complexes were obtained with an excess of hydrogen peroxide as described in Ref. [23]. In the following figures and tables, both species are indicated as heme *d* for the sake of simplicity. In order to avoid denaturation, the Y135A coproheme complex was titrated to 2 eqs. of H_2O_2, whereas the WT heme *b* complex was further titrated to an excess of 1.75 eqs. of H_2O_2. As a result, mass spectrometric data of ferric *Cd*ChdC WT treated with the excess of hydrogen peroxide revealed the presence of about 40% of heme *d*, while for the ferric Y135A about 80% of heme *d* was found upon H_2O_2 titration [10,23].

The Fe(II)-CO adducts at pH 7.0 were prepared by reducing the ferric *Cd*ChdC complexes by addition of a freshly prepared sodium dithionite (20 mg/mL) solution, upon flushing with ^{12}CO or ^{13}CO gas (Rivoira, Milano, Italy), as also described in Ref. [23]. The sample concentration was in the range of 40–70 μM and determined as described previously [13].

2.3. UV–vis electronic absorption spectroscopy

UV–vis electronic absorption spectra were recorded at 298 K, using a 5 mm NMR tube or a 1 mm cuvette by means of a Cary 60 spectrophotometer (Agilent, Santa Clara, CA, USA) with a scan rate of 300 nm min^{-1} and a resolution of 1.5 nm. The UV–vis electronic absorption spectra were measured both before and after RR measurements to ensure that no degradation occurred under the experimental conditions. In all the figures, the absorption spectra were normalized to the intensity of the Soret band and the 450–700 nm region has been further magnified by a factor of 10- or 15-folds, as indicated.

2.4. Resonance Raman (RR) spectroscopy

The resonance Raman (RR) spectra were obtained by excitation with the 413.1 nm line of a Kr^+ laser (Coherent, Innova300C, Coherent, Santa Clara, CA, USA). A cylindrical lens was used to focus the laser beam on the sample, inside a slowly rotating 5 mm NMR tube, and the laser power on the sample was between 1.0 and 5.0 mW, to minimize the CO photolysis of each sample. Backscattered light was collected and focused into a triple spectrometer, working in the subtractive mode. It consists of two SpectraPro 2300i instruments and a SpectraPro 2500i (Acton Research Corp., Acton, MA, USA) instrument, in the final stage, with gratings of 1800 or 3600 grooves/mm, equipped with a liquid nitrogen-cooled CCD detector. A nominal spectral resolution of 1.2 cm^{-1} or 4 cm^{-1} were calculated theoretically based on the optical properties of the spectrometer for the 3600 or the 1800 gratings, respectively.

The RR spectra were calibrated with indene, acetonitrile, and carbon tetrachloride as standards to an accuracy of 1 cm^{-1} for intense isolated bands. All RR measurements were repeated several times under the same conditions to ensure reproducibility. **Table S1** summarizes the integration time and the number of averaged spectra reported in this work. In the figures, all spectra were baseline-corrected and were normalized to the intensity of the ν_4 band at 1370–1372 cm^{-1}. The 1900–2000 cm^{-1} region has been further magnified by a 10-fold factor, if not otherwise indicated in the figures.

The curve-fitting analysis of the spectra was performed by using a spectral simulation program (LabCalc, Galactic Industries, Salem, NH, USA) with a Lorentzian line shape to determine the peak wavenumbers, bandwidths (full width at half maximum) and intensities, with an accuracy of 1 cm^{-1} for the peak positions and the bandwidths. Since some porphyrin bands and the $\nu_{(FeC)}$ of different conformers overlap, the fitting procedure was run iteratively. At first, we fixed only the bandwidths of the better-defined peaks, while the widths of the other bands

were progressively constrained to the same value for the same type of band in all the samples. As a further check, the widths of the less-defined bands were fixed alternatively and were shown to give the same final results. The bandwidths of the $\nu_{(FeC)}$ are 21 cm^{-1}, while for the other porphyrin band they range from 10 to 15 cm^{-1}.

2.5. IR spectroscopy

IR transmission spectra were obtained at 298 K using a FT-IR spectrometer IRaffinity-1 s (Shimadzu, Kyoto, Japan), with a resolution of 4 cm^{-1}. The Fe(II)-CO samples at a concentration of 2 mM were transferred by a vacuum tight syringe to an IR cell (with CaF windows and 50 μm path length) flushed with CO. The buffer solution was used as a reference.

Due to the high concentration required for IR measurements and to the given yield of the expression and purification, it was possible to investigate only the CO adduct of the WT complexed with coproheme.

2.6. Molecular dynamics simulations (MDS)

Initial structures were obtained from Protein Data Bank (PDB IDs: 6XUB and 6XUC) [10]. The heme-*b* charges and bonding parameters were the same as previously published [33–35], which have been extensively tested and validated in conjunction with the Amber force field ff99SB. Coproheme parameters were obtained by a simple modification of heme *b* parameters. Simulation protocol: all MDS were performed using the Amber 20 molecular dynamics simulations package [36]. Initial structure was generated using tleap program. 25,000 steps of steepest descent energy optimization followed by another 25,000 steps of conjugate gradient energy optimization were performed to prevent close contacts. Then 60,000 steps of NVT simulation with a timestep of 0.5 fs, a Langevin thermostat set to a linear ramp from 10 K to 100 K and harmonic restraints over all protein atoms with a spring constant of 1.0 Kcal mol^{-1} $Å^{-2}$. After that, a second NPT thermalization round was performed with a timestep of 1 fs and a temperature ramp going from 100 K to 298 K. After heating, six rounds of equilibrations were performed in the NPT ensemble at 298 K and 1 atm with decreasing restraints with 0.8, 0.6, 0.4, 0.2, 0.1 and 0.05 Kcal mol^{-1} $Å^{-2}$, respectively, where the restraints were applied only to backbone atoms in the last four rounds of equilibration. Production trajectories were obtained in the NPT ensemble using the Berendsen barostat [37] and Langevin thermostat [38], a timestep of 2 fs and a final temperature of 298 K with no additional restraints of any kind. A cutoff for non-bonding interactions of 12 Å and the SHAKE algorithm for constraining light atom bond distances were applied in all the MD simulations. Each production trajectory replica comprised 400 ns with at least two replicas for each of the following cases: WT and H118A, H118F and T172A variants complexed with coproheme and heme *b*. Variants were obtained using tleap program, by simply changing the corresponding amino acid residue during the initial structure building phase. During the addition of CO to the crystal structure of heme and coproheme it was necessary to modify T172 sidechain by rotating its C_a-C_b dihedral angle in order to alleviate a steric clash between T172 methyl group with CO.

3. Results

3.1. UV–vis and RR spectroscopies

In order to probe the heme active site of *Cd*ChdC, we studied the CO adducts of the WT protein and selected variants complexed with coproheme, together with their corresponding complexes obtained upon titration with hydrogen peroxide or hemin reconstitution.

In presence of carbon monoxide, the ferrous proteins bind the exogenous ligand forming a 6-coordinated (6c) low-spin (LS) species, as shown by the electronic absorption UV–vis spectra (**Fig. S1**). The UV–vis spectra of the WT and variants complexed with coproheme are very similar, characterized by a Soret band ranging from 410 to 414 nm, and the Q bands around 534 (Q_{0-1}) and 561 (Q_{0-0}) nm. Upon titration with H_2O_2, only WT and few variants (namely H118A, T172A, N115L and W143F) studied in this work, are active, forming heme *b* [18]. This is confirmed by the overall red-shift of the electronic absorption bands by 6–8 nm (**Fig. S2**) of their CO adducts, due to the conjugation of the double bonds of the newly formed vinyl groups at positions 2 and 4. Accordingly, the RR core size marker bands of the CO adducts of the WT (**Fig. S3**) and variants (data not shown) complexed with coproheme and heme *b* complexes are typical of a 6cLS species. In the heme *b* complex the bending $\delta_{(C\beta CaCb)}$ (data not shown) and $\delta_{(=CH2)}$, and the stretching $\nu_{(C=C)}$ vinyl vibrations are observed. Interestingly, in the CO adduct of the WT heme *b* complex, the two $\nu_{(C=C)}$ vinyl stretching modes, differently from the ferric [13] and ferrous [17] forms, merge into a single band at 1622 cm^{-1}, suggesting that CO binding affects the orientation of the porphyrin and/or the vinyl groups.

3.1.1. WT-CO adducts

The vibrations of the FeCO unit in the WT protein are identified in the RR spectra on the basis of the isotope shift in ^{13}CO versus ^{12}CO ligation (Fig. 2). In both the WT coproheme and heme *b* complexes, two sets of vibrations sensitive to the isotopic substitution have been identified, allowing us to conclude that CO binds the WT in two different conformations.

In the ^{12}CO adducts of WT complexed with coproheme, one conformer, named conformer 1, is characterized by a $\nu_{(FeC)}$ at 503 cm^{-1} and a $\nu_{(CO)}$ at 1952 cm^{-1}. The second conformer, named conformer 2, is characterized by a $\nu_{(FeC)}$ at 515 cm^{-1} and $\nu_{(CO)}$ at 1941 cm^{-1}. The assignment of the $\nu_{(FeC)}$ / $\nu_{(CO)}$ couple vibrations has been made according to their wavenumber inverse correlation. This depends on the polar interaction strengths with distal residues [30,31]. The pairing of the FeC and CO stretching in the WT is further supported by the data obtained in the variant proteins (vide infra). The presence of the two bands at 1941 and 1952 cm^{-1} were also confirmed by IR spectroscopy (**Fig. S4**).

Moreover, a weak band at 582 cm^{-1} (563 cm^{-1} in the ^{13}CO adducts) in the RR spectra is assigned to the $\delta_{(Fe\text{-}C\text{-}O)}$ bending mode of conformer 2 (Fig. 2). DFT calculations revealed that this latter mode is an out-of-phase combination of Fe–C–O bending and Fe—C tilting [39]. Since this bending mode is only revealed in a few heme proteins and is not observed in protein-free heme adducts, its RR intensity can be considered an indicator of off-axis interactions, between CO and with nearby residues. These interactions can be either steric or, more likely, electrostatic [40]. Furthermore, the wavenumber of this bending mode is correlated with that of the $\nu_{(FeC)}$, but the observed change in the $\delta_{(Fe\text{-}C\text{-}O)}$ is usually small [41].

Formation of heme *b* either upon addition of hydrogen peroxide or hemin reconstitution lead to the same results for the CO adduct of the WT (data not shown) and alters the wavenumber of the vibrational modes corresponding to the CO conformers with respect to coproheme. In fact, conformer 1 is characterized by a $\nu_{(FeC)}$ at 498 cm^{-1} and $\nu_{(CO)}$ at 1959 cm^{-1}, and conformer 2 by a $\nu_{(FeC)}$ at 507 cm^{-1} and $\nu_{(CO)}$ at 1945 cm^{-1} in the heme *b* complex. Also, in this latter species, a $\delta_{(Fe\text{-}C\text{-}O)}$ bending mode is found at 580 cm^{-1} (Fig. 2).

Since in both the CO adducts of the WT *Cd*ChdC complexed with coproheme and heme *b*, the two $\nu_{(FeC)}$ stretching modes are overlapped, we confirmed their presence by spectral deconvolution. The curve-fitting analysis of the ^{13}CO versus ^{12}CO RR spectra in the low wavenumber region of the coproheme and heme *b* complexes are compared in Fig. 3. The four spectra are characterized by porphyrin bands, whose wavenumbers do not change upon isotopic substitution: in the coproheme complexes, the bands at 471, 490, 526, 546, and 562 cm^{-1} are assigned to ν_{33}, γ_{22}, γ_{12}, ν_{49}, and γ_{21}, respectively, and in the heme *b* complexes the bands at 486, 520, 547, 565 cm^{-1} are assigned to γ_{22}, γ_{12}, ν_{49}, and γ_{21}, respectively [42,43]. The only bands of the carbon monoxide adducts, which down-shift when ^{13}CO is replaced with ^{12}CO, are

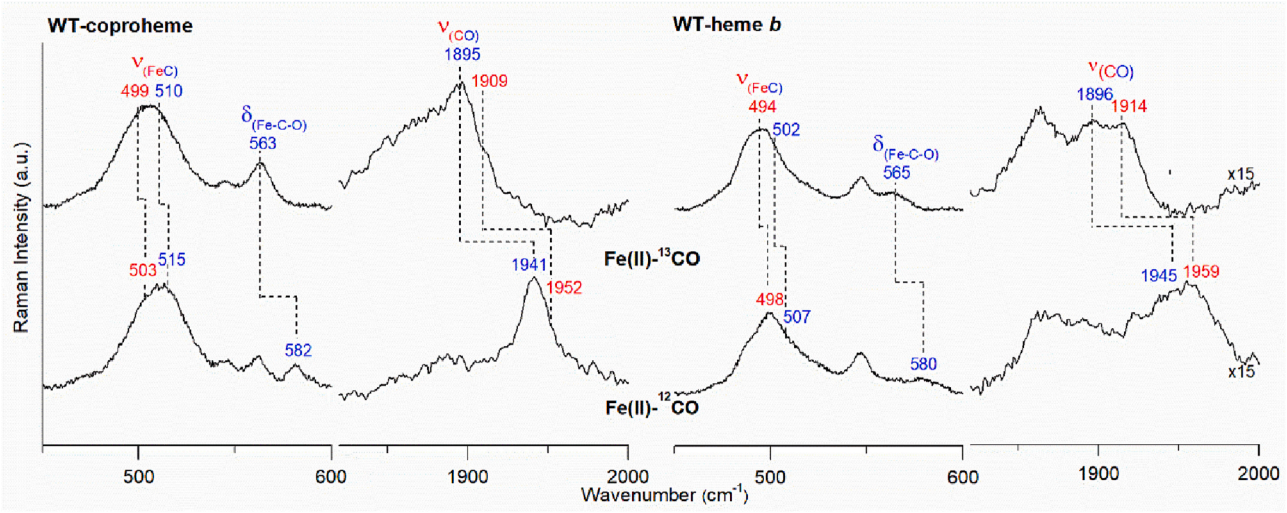

Fig. 2. RR spectra in the low and high wavenumber regions of the CO adducts of the WT *Cd*ChdC complexed with coproheme (left) and heme *b* (right). The wavenumbers of the FeCO vibrations are identified on the basis of the isotope shift in ^{13}CO (top) versus ^{12}CO (bottom) ligation and indicated in red for conformer 1 and in blue for conformer 2. (For interpretation of the references to colour in this figure legend, the reader is referred to the web version of this article.)

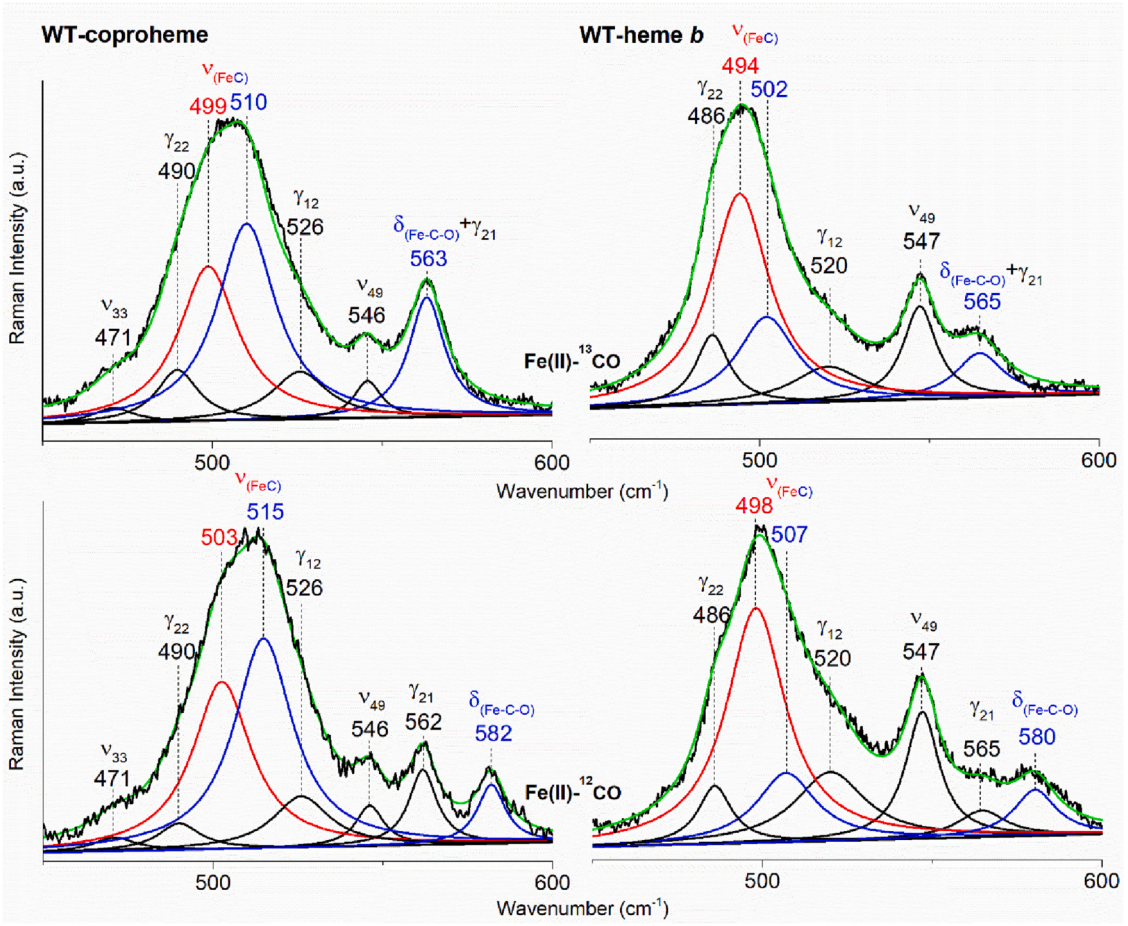

Fig. 3. Curve-fitting analysis of the RR spectra in the low wavenumber region of the ^{13}CO and ^{12}CO adducts of the WT *Cd*ChdC complexed with coproheme (left) and heme *b* (right). The wavenumbers of the FeCO vibrations are indicated in red for conformer 1 and in blue for conformer 2. The bands indicated in black at 471, 490, 526, 546 and 562 cm^{-1} in the coproheme complex, and at 486, 520, 547 and 565 cm^{-1} in the heme *b* complex are assigned according to Refs. [42, 43]. (For interpretation of the references to colour in this figure legend, the reader is referred to the web version of this article.)

those assigned to the stretching modes of the FeCO unit, as reported in Table 1.

3.1.2. *The role of the distal H118 residue*

In the actinobacterial *Cd*ChdC, a distal H118 acts as a distal base for deprotonation and subsequent heterolytic cleavage of hydrogen

Table 1
Wavenumbers (cm^{-1}) of the FeCO vibrations as observed in the CO adducts of WT and selected variants of *Cd*ChdC complexed with coproheme, MMD, heme *b* and heme *d*.

	Conformer 1		Conformer 2		
	$\nu_{(FeC)}$	$\nu_{(CO)}$	$\nu_{(FeC)}$	$\nu_{(CO)}$	$\delta_{(Fe\text{-}C\text{-}O)}$
WT-coproheme	503	1952	515	1941	582
T172A-coproheme	503	1952	515	1941	582
H118A-coproheme	500	1954			
H118F-coproheme	503	1952			
W143F-coproheme	503	1952	515	1942	582
R208L-coproheme	501	1951	515	1942	
N115L-coproheme	501	1952	515	1942	580
R139L-coproheme	497	1961	515	1942	
Y135A-coproheme			511	1938	582
WT-heme b	498	1959	507	1945	580
T172A-heme b	497	1962	507	1945	579
H118A-heme b	497	1959			
H118F-MMD	501	1953			
H118A-reversed heme b	495	1955			
WT-heme d	494	1965			
Y135A-heme d	496	1965			
W143F-heme b	498	1959	507	1945	580
N115L-heme b	498	1962	507	1945	580

peroxide [10] in a concerted action with the catalytic Tyr (Y135), leading to a high reactivity of *Cd*ChdC toward H_2O_2.

As shown in Fig. 4 **(left)**, in WT *Cd*ChdC complexed with ferric coproheme (PDB ID: 6XUC) [10], the distal H118 residue is stabilized by H-bonds with the propionate at position 7 (p_7) via the N_δ, and with the T172 residue via the N_ε. Moreover, this latter nitrogen is sitting on the top of the heme iron at a distance of 5.1 Å.

In order to evaluate whether this conserved H118 residue is capable to interact with exogenous ligands, such as carbon monoxide, and the possible effects on the CO ligation, we have characterized the CO adducts of H118A, H118F, and T172A variants, before and after titration with H_2O_2 or hemin reconstitution. Their RR spectra are compared in Fig. 5 and the corresponding curve-fitting analysis are reported in **Fig. S5**.

The vibrational bands of the FeCO unit ascribed to conformer 2 disappear in the H118A variant, where only conformer 1 is observed. This indicates that in both the WT coproheme and heme *b* complexes, the CO in conformer 2 is H-bonded to the N_ε of H118. Accordingly, only conformer 1 is found in the H118F variant as well. It is worth noticing that in this latter variant upon addition of H_2O_2, the vibrations characteristic of conformer 1 remain almost identical to the ones of the coproheme complex (Fig. 5). In fact, H118F is able to catalyze only the MMD reaction intermediate species, since the 90° rotation before the p_4 decarboxylation is inhibited by the steric hindrance of the bulky Phe residue [10,13].

Moreover, in the T172A variant, where, according to the X-ray structure, the H-bond between T172 and H118 is missing, reversed relative intensities of the $\nu_{(FeC)}$ stretching modes of the two conformers are observed as compared to the WT (Fig. 5). These results, confirmed by curve-fitting analysis (**Fig. S5**), suggest a destabilization of conformer 2. In fact, as reported in Ref. [44], while the $\nu_{(FeC)}$ relative intensity can be used to evaluate the relative CO populations, the intensity profiles of the corresponding $\nu_{(CO)}$ as measured in the RR spectra are quite different from the corresponding bands measured by IR spectroscopy. As a consequence, the authors concluded that "both $\nu_{(FeC)}$ (as measured by Raman spectroscopy) and $\nu_{(CO)}$ (as measured by infrared spectroscopy) can be used to monitor changes in the CO-bound protein populations" [44].

Since both conformers are still present and their CO vibrations wavenumbers are not affected by mutation, these results indicate that the T172 residue is not directly involved in the CO binding. In addition, upon H_2O_2 titration, the heme *b* complex of T172A remains very similar to the WT. The different effect on the coproheme and heme *b* complexes suggests that after the 90° degree rotation of the porphyrin within the protein pocket, both the binding and stabilization of the bound CO by the distal residues are very limited.

On the other hand, as previously reported [17], the distal H118 also plays an important role in heme *b* binding. In fact, the WT heme *b* complex either obtained by hemin reconstitution or hydrogen peroxide titration is almost identical either in the ferric or ferrous forms and in the CO adducts (see above). Conversely, the access of heme *b* into the protein cavity can be prevented by the sterically encumbered Phe residue (H118F), while its substitution with the small apolar Ala residue (H118A) favors the insertion of heme *b* in a reversed conformation along the α-γ *meso* axis [17]. We found that, unlike the case of reversed myoglobin (Mb) where neither the proximal nor the distal Fe-ligand binding are affected by the rotational heme disorder [45,46], in the H118A variant the Fe-proximal His bond was strengthened [17].

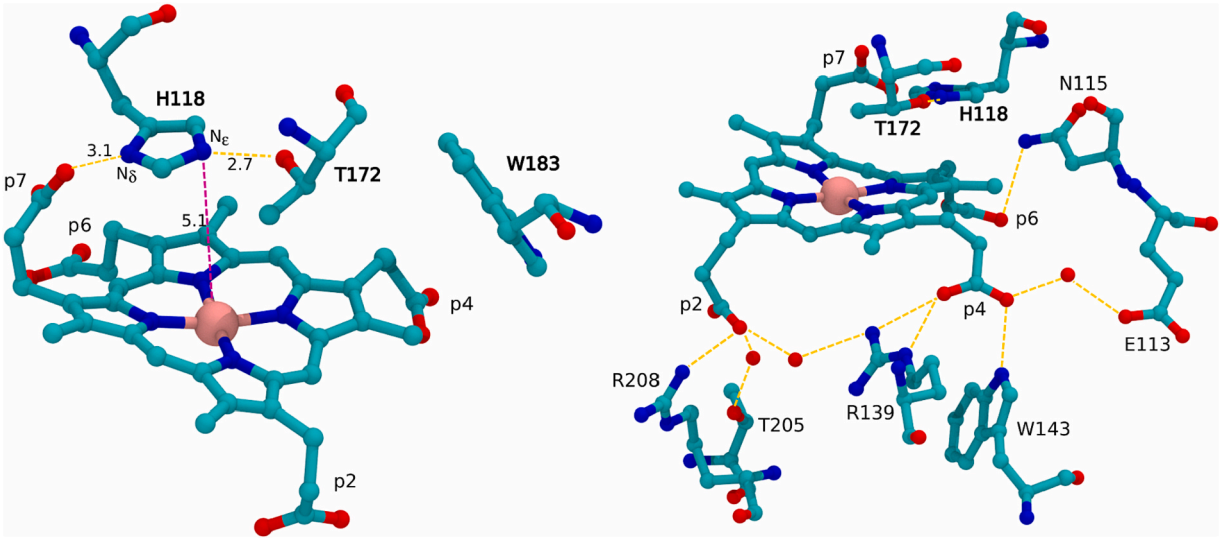

Fig. 4. Structure of the active site of the WT *Cd*ChdC complexed with ferric coproheme (PDB ID: 6XUC) [10], showing the H-bonds distances (in Å). Left: H-bonds between $N_{\delta\ (H118)}$ and p_7, and between $N_{\varepsilon\ (H118)}$ and T172. The distance between $N_{\varepsilon\ (H118)}$ and the Fe atom is also shown (magenta dashed line). Right: H-bonds involving p_2, p_4, and p_6. Red spheres indicate water molecules, while H-bond interactions are shown as yellow dashed lines. (For interpretation of the references to colour in this figure legend, the reader is referred to the web version of this article.)

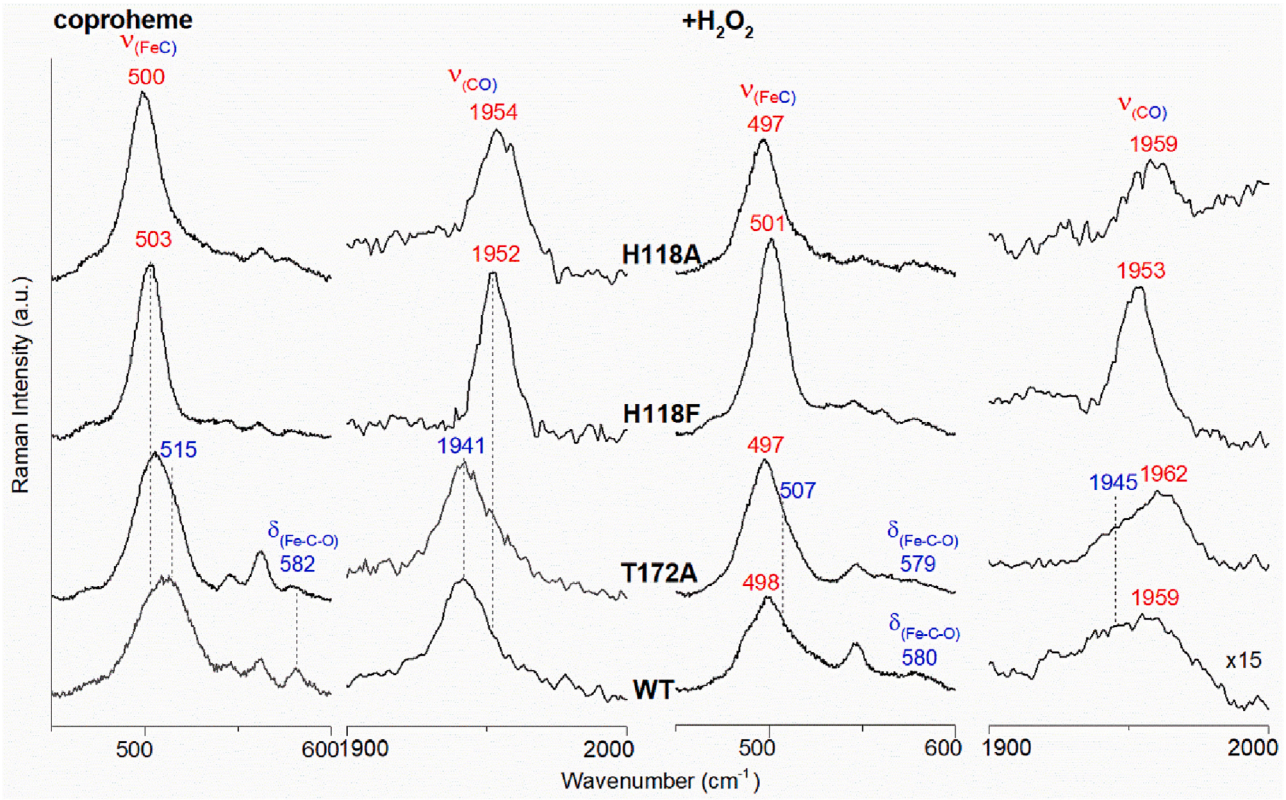

Fig. 5. RR spectra in the low and high wavenumber regions of the CO adducts of the WT and selected variants of *Cd*ChdC complexed with coproheme before (left) and after (right) hydrogen peroxide titration. The wavenumbers of the FeCO vibrations are indicated in red for conformer 1 and in blue for conformer 2. (For interpretation of the references to colour in this figure legend, the reader is referred to the web version of this article.)

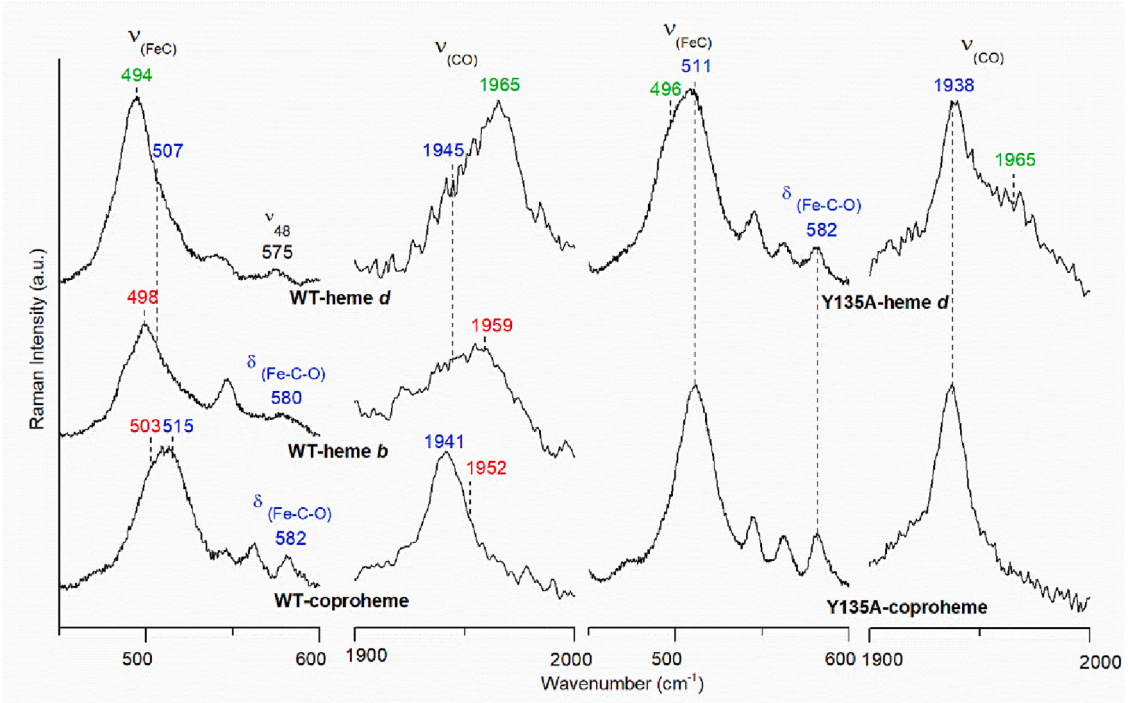

Fig. 6. RR spectra in the low (left) and high (right) wavenumber regions of the CO adducts of the WT and selected variants of *Cd*ChdC complexed with coproheme, heme *b* and heme *d*, respectively. The wavenumbers of the FeCO vibrations are indicated in red for conformer 1, in blue for conformer 2, and in green for heme *d*. (For interpretation of the references to colour in this figure legend, the reader is referred to the web version of this article.)

Therefore, with the aim to evaluate the effect of the reversed heme insertion on the distal site ligand stabilization, we extended the study probing the CO binding on the H118A hemin-reconstituted variant (H118A-reversed). The spectra of the H118A-CO adduct of the hemin reconstituted or hydrogen peroxide titrated protein are not identical, differently from what observed for the WT (**Figs. S2 and S6**). Upon reconstitution the UV–vis electronic absorption spectrum upshifts by 3–4 nm and, in the RR spectra, the vinyl groups give rise to different stretching and bending vibrations with respect to the complex obtained by H_2O_2 titration. In addition, conformer 2 is characterized by slightly different $\nu_{(FeC)}$ and $\nu_{(CO)}$ wavenumbers (at 495 and 1955 cm^{-1}, respectively) with respect to the complex obtained by H_2O_2 titration (at 497 and 1959 cm^{-1}, respectively).

Recently, we also found that the distal H118 is involved in the oxidation of the porphyrin ring in the presence of hydrogen peroxide. We have shown that the actinobacterial *Cd*ChdC in presence of an excess of H_2O_2 could generate new species. In particular, this form has been detected in the Y135A variant complexed with coproheme, which is catalytically inactive, when titrated with H_2O_2 and in the WT heme *b* complex, upon additional titration with hydrogen peroxide after the product formation [23]. In both cases, H_2O_2 causes a porphyrin hydroxylation of ring C or D, compatible with the formation of an iron chlorin-type heme *d* species [21]. This conversion requires the presence of the distal H118, since the H118A, H118F single, and the Y135A/H118F double variants are not altered by an excess of hydrogen peroxide. Therefore, we have further investigated the CO adducts of these side-product species in both the WT and Y135A variant in order to study whether the hydroxylation of the porphyrin affects the binding and distal stabilization of exogenous ligands.

The Y135A variant differs from the WT since only conformer 2 is observed in its coproheme complex, with the at 511 and 1938 cm^{-1}, respectively (Fig. 6). Upon addition of hydrogen peroxide this species decreases and the coproheme *d* - CO adduct is observed, characterized by $\nu_{(FeC)}$ and $\nu_{(CO)}$ at 496 and 1965 cm^{-1}, respectively. In the WT heme *b* complex an excess of hydrogen peroxide causes a decrease of the intensity of the bands of conformer 1, and the newly formed heme *d* -CO adduct is characterized by $\nu_{(FeC)}$ and $\nu_{(CO)}$ at 494–1965 cm^{-1}, respectively. These results are in agreement with the mass spectrometric data which showed, for the corresponding ferric forms, a mixture of coproheme *d* and heme *d* together with their precursors (coproheme for ferric Y135A or heme *b* for WT) [10,23]. However, the hydrogen-bonded CO adduct (conformer 1) is only weakly affected by the excess of H_2O_2. In the UV–vis spectra both the coproheme *d* and heme *d* CO adducts are characterized by a new band at about 609–610 nm [23]. The overall data are in agreement with the CO adducts of chlorins [47,48].

3.1.3. *Effect of the propionate H-bonds on CO binding*

The crystal structure clearly shows that an extensive H-bond network involving the propionate groups of the porphyrin with water molecules and specific amino acid residues strongly stabilizes the active site of the WT *Cd*ChdC complexed with coproheme (PDB ID: 6XUC) [10] (Fig. 4, **right**). Recently, we have studied the role of these H-bonds in solution, by characterizing the RR and UV–vis spectra of several single and double variants of *Cd*ChdC (lacking the H-bonds with the propionate groups) complexed with coproheme and heme *b*. Based on these results, we dug out the role of each H-bond not only in the stabilization of the coproheme inside the active site before and after the catalytic reaction, but also on the protein activity. We found that the rupture of the H-bonds with p_6 (N115L) or p_7 (H118A, T172A) does not destabilize the porphyrin ring inside the cavity and does not alter the protein reactivity toward hydrogen peroxide. On the contrary, the H-bond interactions involving p_2 and p_4 are fundamental for the stability of the porphyrin ring in the pocket and for maintaining the proper propionate orientations to allow their decarboxylation by the Y135 catalytic residue [18].

Since propionates are known to play a role in the selective recognition of exogenous ligands and to regulate the access to the substrate-binding site of heme proteins [49–51], here we have evaluated the influence of the disruption of the extensive H-bond network in the heme pocket of *Cd*ChdC on CO binding. Therefore, we investigated the CO adducts of the variants, whose mutation involve the rupture of the H-bonds with p_2 (R208L), p_4 (W143F), p_2 and p_4 (R139L), and p_6 (N115L) (Fig. 7). Among these variants, only W143F and N115L react with hydrogen peroxide to form heme *b* and both their products bind CO in a similar manner to the WT (**Fig. S7**).

On the contrary, in the CO adducts of the coproheme complexes different effects are observed for the variants (Fig. 7**).** The elimination of the H-bonds with p_4 or p_6 has relatively small consequences on the CO binding. The rupture of the H-bond between W143 and p_4 (W143F) does not alter CO binding, the spectra are identical to the WT, while in the N115L variant, the equilibrium between conformers 1 and 2 is reversed, as shown by the relative intensities of their CO vibrations in the RR spectra. On the contrary, marked changes are observed for R208L and R139L variants, in agreement with the destabilization of the active site pocket, observed in their ferric forms [18]. In both R208L and R139L, the interaction between the CO and the distal H118 residue is impaired, since conformer 1 becomes predominant. Moreover, in the R139L variant the $\nu_{(FeC)}$ and the $\nu_{(CO)}$ stretching vibrations of conformer 1 shift to 497 and 1961 cm^{-1}, respectively. It is worth mentioning that the effect of the elimination of the H-bond with p_7 cannot be disentangled spectroscopically, as it is coupled to the removal of the distal H118 residue.

3.2. *Molecular dynamics simulations*

The initial structure for MD simulations was built from the crystal structure (PDB ID: 6XUC) [10]. However, when adding CO we found a strong steric clash between CO and the T172 methyl group (Fig. 8, panel A). To allow the carbon monoxide to fit in, we had to modify T172

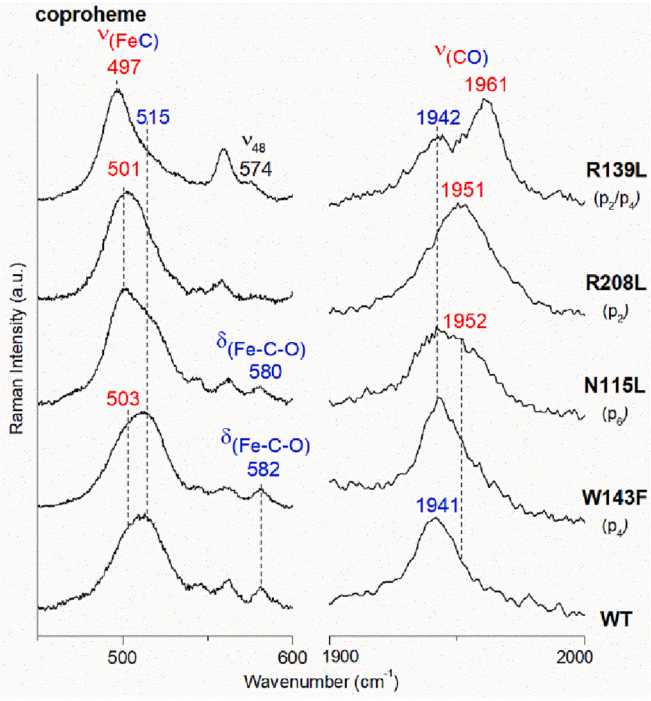

Fig. 7. RR spectra in the low (left) and high (right) wavenumber regions of the CO adducts of WT *Cd*ChdC and selected variants complexed with coproheme. The wavenumbers of the FeCO vibrations are indicated in red for conformer 1 and in blue for conformer 2. The propionates, whose H-bond are removed by mutation, are reported in black in brackets. (For interpretation of the references to colour in this figure legend, the reader is referred to the web version of this article.)

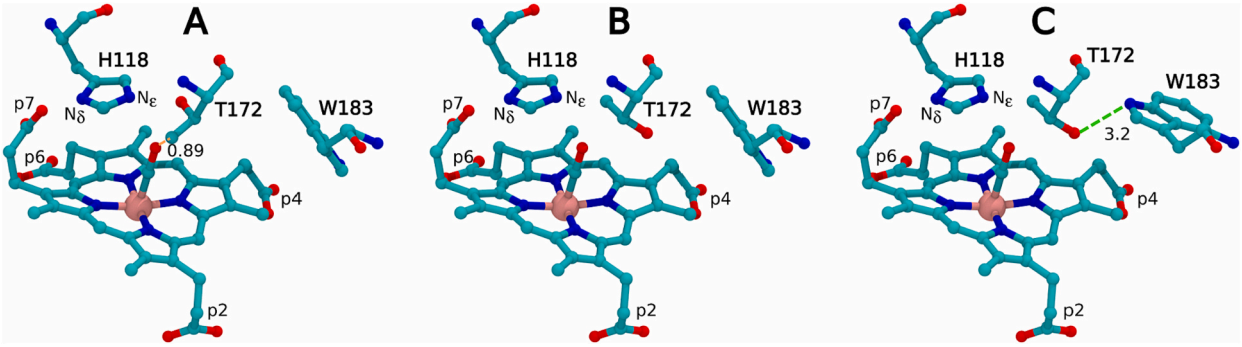

Fig. 8. Representation of the active site of WT *Cd*ChdC complexed with coproheme. Panel A: Crystal structure with added CO, showing the steric clash between T172 and carbon monoxide with an O_{CO}-C_{T172} distance of 0.89 Å. Panel B: Modified structure with T172 side chain rotated along the C_a-C_b to avoid CO-T172 steric clash. Panel C: MD initial structure with the modified W183 conformation to facilitate a W183-T172 H-bond.

conformation by rotating its side chain along the C_a-C_b axis to alleviate the steric clash, as shown in Fig. 8, panel B. We also built an additional initial structure with a further modification of W183 conformation allowing this residue to be able to form an H-bond with T172 (Fig. 8**,** panel C).

3.2.1. *Wild-type*

We performed a MDS of the WT *Cd*ChdC coproheme complex (1.0 μs), using the initial structures corresponding to Fig. 8, panel B, monitoring possible H-bonding interactions between CO and H118 or T172, H118 and T172, and T172 and W183. The distance distributions sampled along the simulation are shown in Fig. 9, **left**. A strong H-bond between CO and H118 is observed along most of the simulation. Interestingly, the H-bond between H118 and T172, observed in the crystal structure of the ferric unligated protein is formed only for a small fraction of the time scale of the simulation (red line in Fig. 9, **left**). Moreover, by analyzing the time series for the same distances (**Fig. S8**) we found a clear correlation between H118-T172 and T172-CO interactions since T172 is also able to establish an interaction with CO, only when H118 is H-bonded to T172. As reported above, the H-bond between H118 and CO is observed along the whole time scale of the simulation, regardless of the T172 interactions.

3.2.2. *H118A and H118F variants*

Simulations of the H118A variant using the initial structures corresponding to Fig. 8 (panel B) lead to results inconsistent with the Raman experiments. Namely, a strong H-bond between the CO and T172 is observed during the time scale of 1.2 μs simulations (see supplementary information, **Fig. S9**), while the RR experiments suggest only a modest polar interaction between the bound CO and the distal cavity. On the other hand, the simulations performed using the initial structure depicted in Fig. 8 (panel C) turned out to be stable along 800 ns of simulation, suggesting that this conformation may be significantly populated in solution. Results for selected distances in this simulation are shown in Fig. 9, **right**. In fact, a very strong W183-T172 H-bond is established (corresponding to the sharp peak of the W183-T172 distance centered at 3 Å depicted as a yellow line in Fig. 9, **right**) which competes very effectively with the T172-CO interaction to the point that the latter is not relevant, consistently with the Raman experiments.

As a control, we also performed simulations for the WT (1.2 μs) using this initial structure (shown in Fig. 8**,** panel C). Simulations were stable and compatible with those presented in Fig. 9, **left** and with the experiments (data not shown).

3.2.3. *T172A variant*

The distance probability distributions of the H118-CO H-bond in the

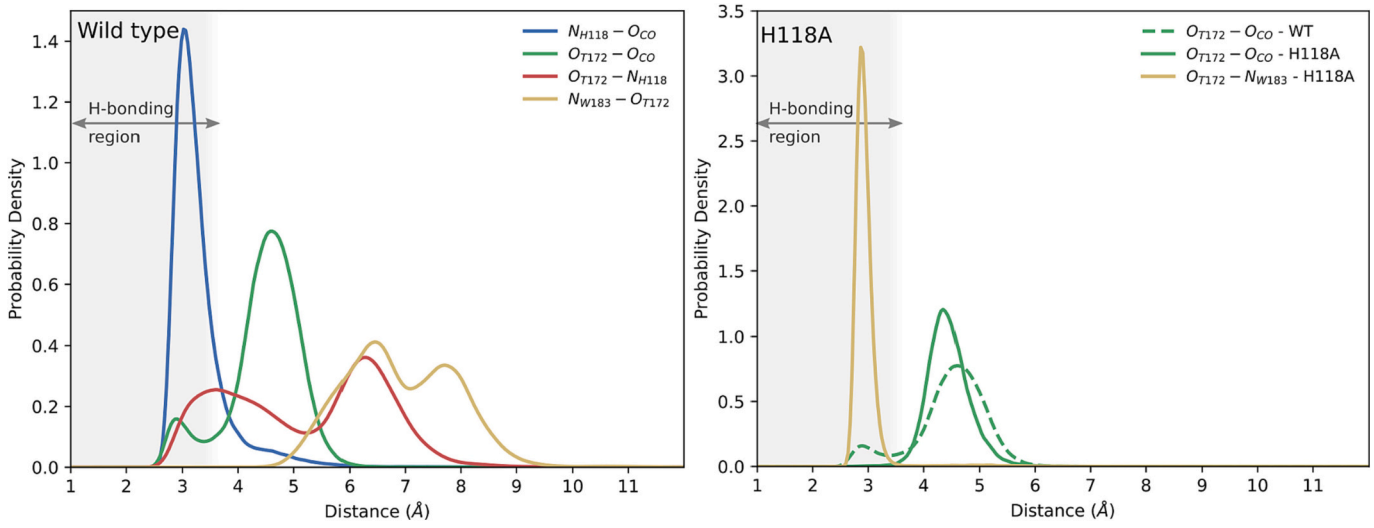

Fig. 9. Distance distribution for N_{H118}-O_{CO}, O_{T172}-O_{CO}, N_{H118}-O_{T172} and O_{T172}-N_{W183} coordinates in MDS of *Cd*ChdC coproheme complexes. Left: Wild type. The strong interaction between H118 and T172 seen in the crystal structure is broken in the presence of CO. Right: H118A variant MDS with initial structure with W183 in modified conformation (Fig. 8, panel C). No interaction between T172 and CO is observed in H118A mutant (green solid lines). The O_{T172}-O_{CO} distance for WT is shown for comparison (green dashed line). A strong H-bond between W183 and T172 is found along the time scale of the simulation (yellow solid line). (For interpretation of the references to colour in this figure legend, the reader is referred to the web version of this article.)

T172A variant of the *Cd*ChdC coproheme complex as obtained by MDS (1.6 μs) is shown in **Fig. S10** in comparison to the WT. The maximum probability distance is 3 Å, similar to the native protein. However, in the T172A variant the population of the H-bonded conformation is reduced, and the probability density extends up to much longer distances as compared to the WT. This is consistent with the Raman results that show in the T172A-CO adduct a larger population for the non H-bonded conformation (conformer 1) with respect to the H-bonded one (conformer 2).

3.2.4. *CdChdC heme b complexes*

Simulations for *Cd*ChdC heme *b* complexes of WT and variants were also performed. We found that the *Cd*ChdC heme *b* complex was significantly more flexible than its *Cd*ChdC coproheme counterpart, and accordingly, no converged distance probability results can be extracted from a 1 μs simulation.

4. Discussion

Our findings show how CO binding is affected by mutations of key residues of the active site of the coproheme decarboxylase enzyme from actinobacterial *Cd*ChdC. In order to rationalize these results, we report in a plot the $\nu_{(FeC)}$ versus $\nu_{(CO)}$ stretching mode wavenumbers of WT and selected variants of *Cd*ChdC complexed with coproheme, before and after titration with hydrogen peroxide (Fig. 10). For the sake of clarity, the data regarding the variants (Table 1), where the FeCO vibrations wavenumbers are almost identical to those of the WT, although with a change in their relative populations (namely T172A, N115L, W143F and R208L), are not reported in the plot.

The $\nu_{(FeC)}$ and $\nu_{(CO)}$ wavenumbers of the CO adducts of heme proteins and model compounds containing a His residue as the fifth iron ligand are inversely correlated and their position along the correlation line depends on the strength of polar interactions with distal residues [30,31]. Moreover, increasing the strength of the trans-axial ligand of CO, the $\nu_{(FeC)}$ wavenumber decreases as a consequence of σ competition. This effect results in another $\nu_{(FeC)}$ versus $\nu_{(CO)}$ correlation line lying below the one corresponding to heme proteins with a proximal His residue as fifth iron ligand [31].

CO binds the WT coproheme complex, giving rise to two conformers. Conformer 2 corresponds to a more polar interaction than conformer 1, as indicated by their positions in the $\nu_{(FeC)}$ versus $\nu_{(CO)}$ correlation plot. The bound CO is stabilized by an H-bond interaction with the distal H118 amino acid, since conformer 2 disappears upon replacement of the H118 residue with nonpolar residues (H118A and H118F variants), a conclusion supported by MDS. Accordingly, both the H118 variants are characterized by only one conformer, whose vibrational signatures are very similar to those of the WT conformer 1 (Fig. 10**, left**).

MDS clearly indicate that in the T172A variant the mutation reduces the interaction probability between H118 and CO, as highlighted by the strong increase of the population of conformer 1 at the expense of conformer 2 when compared to WT. This change is not, however, caused by the missing H-bond between T172 and H118, as suggested by the ferric crystal structure, since in the WT CO adduct this interaction between T172 and H118 is not significant (Fig. 9, **left**). Therefore, the overall H-bond network of the active site is involved in the equilibrium between the two CO conformations. Interestingly, MDS also show that, differently from the T172-H118 H-bond interaction found in the ferric WT-coproheme crystal structure, T172 forms a strong H-bond with W183 (Fig. 9**, right**) upon carbon monoxide ligation. Given the close position of T172 to CO, this interaction prevents the stabilization of CO by the T172, which is in agreement with the RR experiments. Previous studies by Liu et al. [16] suggested an important role for an analogous Trp residue (W198 in *Gs*ChdC, which corresponds to W183 in *Cd*ChdC). W198, together with W157 (corresponding to W143 in *Cd*ChdC) was found to form a "gate" construction that regulates the rotation of the MMD during the enzyme's catalytic cycle. Interestingly, the side chain of W198 in *Gs*ChdC is in a conformation more similar to our modified W183 than in the native crystal structure of *Cd*ChdC. In this context, the strong W183 -T172 interaction in the H118A variant of *Cd*ChdC coproheme complex might indicate a possible role for the W183 residue, similar to that suggested for W198 in *Gs*ChdC. As a control, we also performed additional MDS of the ferric WT *Cd*ChdC coproheme complex without CO (**Fig. S11**). One MDS has been performed starting from the crystal structure (PDB ID: 6XUC) [10] without modifications (**panel a**), the other from the same crystal structure with the modified W183 conformation (**panel b**), as in Fig. 8, (T172 has not been modified, since carbon monoxide is not present). The former MDS showed a very strong H118-T172 H-bond in agreement with the crystal structure, while the latter simulation shows that T172 is able to form strong H-bonds with H118 or W183 (**panels c and d**). These results suggest that this alternative W183 conformation might be also significantly populated in solution in absence of CO.

The WT heme *b* complex binds CO in two different conformations, but both conformers downshift on the correlation line, as compared to those of the coproheme complex (Fig. 10**, right**). Therefore, upon conversion to heme *b*, i.e. after the decarboxylation of both propionates p_2

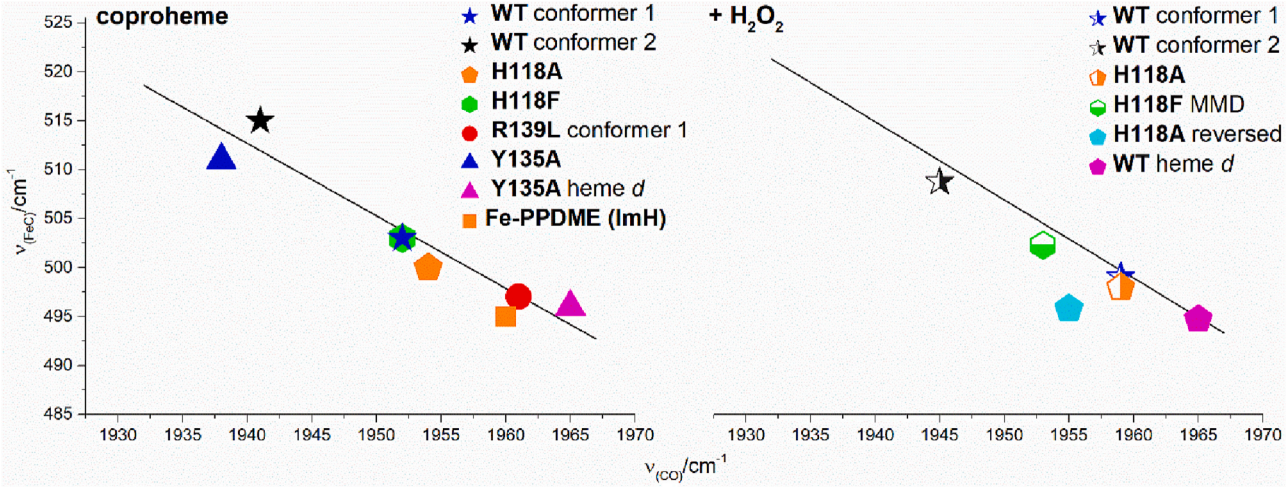

Fig. 10. Back-bonding correlation of the $\nu_{(FeC)}$ and $\nu_{(CO)}$ stretching wavenumbers of the CO adducts of WT, H118A, H118F, R139L and Y135A variants of *Cd*ChdC complexed with coproheme before (left) and after (right) hydrogen peroxide titration. The line has been obtained according to Ref. [31]. Data for imidazole adduct of ferrous protoporphyrin IX dimethyl ester (Fe-PPDME (ImH)) are also reported [52].

and p_4 to v_2 and v_4, and the rotation by 90° of the porphyrin ring inside the cavity, the exogenous CO probes a less polar cavity. However, conformer 2 is still interacting with the distal H118, since it disappears in the H_2O_2-titrated H118A heme *b* complex. In this variant the vibrational features of the only observed CO conformer almost coincide with those of the WT conformer 1. On the contrary, conformer 1 of the reversed H118A (hemin reconstituted) lies slightly below the correlation line, probably as a consequence of a small trans-axial effect, in agreement with the strengthening of the Fe-Im stretching mode found in the reversed ferrous form in comparison to the H_2O_2-titrated H118A heme *b* [17].

Different is the behavior of the H118F variant. Due to the bulky and hydrophobic Phe ring, the catalytic reaction stops at the formation of the unrotated MMD reaction intermediate, which differs from the coproheme only for the presence of a vinyl in position 2. Accordingly, the CO binds to MMD similarly to its corresponding coproheme complex. This confirms that only after the 90° rotation of the porphyrin within the active site, the CO experiences a much less polar environment.

The effect of the simultaneous rupture of the H-bond interactions with both p_2 and p_4 in the R139L variant can be clearly observed in the correlation plot (Fig. 10**, left**). The mutation of this residue, conserved in actinobacterial ChdCs, alters the architecture of the distal cavity since conformer 1 downshifts along the correlation line to the region characteristic of CO with no polar interactions. These results suggest the presence of an open cavity, reminiscent of that found for the imidazole adduct of ferrous protoporphyrin IX dimethyl ester ($\nu_{(FeC)}$ at 495 cm^{-1} and $\nu_{(CO)}$ at 1960 cm^{-1}) [52]. The data are in agreement with the finding that in the ferric form of this variant a severe reorganization of the active site occurs as well [18].

Furthermore, the effect of the mutation of the redox-active Y135 residue to Ala is to strengthen the distal carbon monoxide interaction, being the Y135A coproheme complex characterized by only one CO conformer (Fig. 10**, left**), slightly shifted below the $\nu_{(FeC)}$ versus $\nu_{(CO)}$ correlation line, as compared to the WT conformer 2. This minor trans-axial effect agrees with previous reports [23], showing a strengthening of the Fe-Im stretching mode in the ferrous Y135A coproheme complex with respect to the native protein.

The CO adducts of chlorins (e.g. heme *d*) were reported to be described by the same $\nu_{(FeC)}$ versus $\nu_{(CO)}$ correlation line of heme *b* proteins [47,48]. In *Cd*ChdC, conversion to a (copro)heme *d*-CO species upon addition of an excess of hydrogen peroxide to either the Y135A coproheme (Fig. 10**, left**) or WT heme *b* complexes (Fig. 10**, right)** leaves the FeCO unit in a completely nonpolar environment. This is typical of an open distal pocket conformation similar to that observed in both myoglobin CO and horseradish peroxidase CO adducts at pH 3, and consistent with the distal His side chain swung out of the heme pocket [40,44,53–55].-

4.1. Comparison with firmicutes

The vibrational features of the CO adducts of the actinobacterial WT *Cd*ChdC with those of firmicute *Lm*ChdC and *Sa*ChdC complexed with coproheme and heme *b* are compared in Fig. 11. Firmicutes lack the distal histidine 118 residue, but contain a glutamine residue (namely Q185 in *Sa*ChdC and Q187 in *Lm*ChdC) capable of interacting with CO [19].

*Lm*ChdC and *Sa*ChdC were shown to be characterized by a single conformer when bound to CO, both in complex with the substrate (coproheme) and the product (heme *b*). In the CO adducts of the coproheme complexes (Fig. 11**, left**), the *Cd*ChdC conformer 2 is very similar to that of the *Sa*ChdC CO adduct ($\nu_{(FeC)}$ at 513 and $\nu_{(CO)}$ at 1941 cm^{-1}), characterized by a moderate H-bond donation or electrostatic interaction between the bound carbon monoxide and the distal Q185 residue [15]. While in the *Lm*ChdC the CO interaction with the Q187 residue is weaker ($\nu_{(FeC)}$ at 508 and $\nu_{(CO)}$ at 1947 cm^{-1}) than in *Cd*ChdC conformer 2, but still stronger than that observed for *Cd*ChdC conformer 1 [56]. On the contrary, the heme *b*-CO adducts of the firmicute ChdCs (Fig. 11**, right**) give rise to RR spectra very similar ($\nu_{(FeC)}$ at 500 and $\nu_{(CO)}$ at 1960 cm^{-1} in *Lm*, and $\nu_{(FeC)}$ at 498 and $\nu_{(CO)}$ at 1958 cm^{-1} in *Sa*) to those of the *Cd*ChdC conformer 1, characterized by low polar interactions with the distal residues. In the firmicute ChdCs, after the 90° rotation of the porphyrin ring within the active site, which follows the decarboxylation of p_2 to v_2, CO does not interact with the distal cavity, while in *Cd*ChdC the H118 residue is still capable to stabilize the bound CO, although with a much weaker interaction than in the coproheme pose.

5. Conclusions

The results confirm the fundamental role played by the distal H118, a unique characteristic of the actinobacterial coproheme decarboxylases, for the coproheme complex in the stabilization of the incoming exogenous ligand. The findings that: i) upon titration the heme *b* CO adduct of T172A remains identical to the WT, ii) in all heme *b* complexes the interaction between CO and the distal H118 is much weaker than in their coproheme counterparts, suggest that after the decarboxylation and the

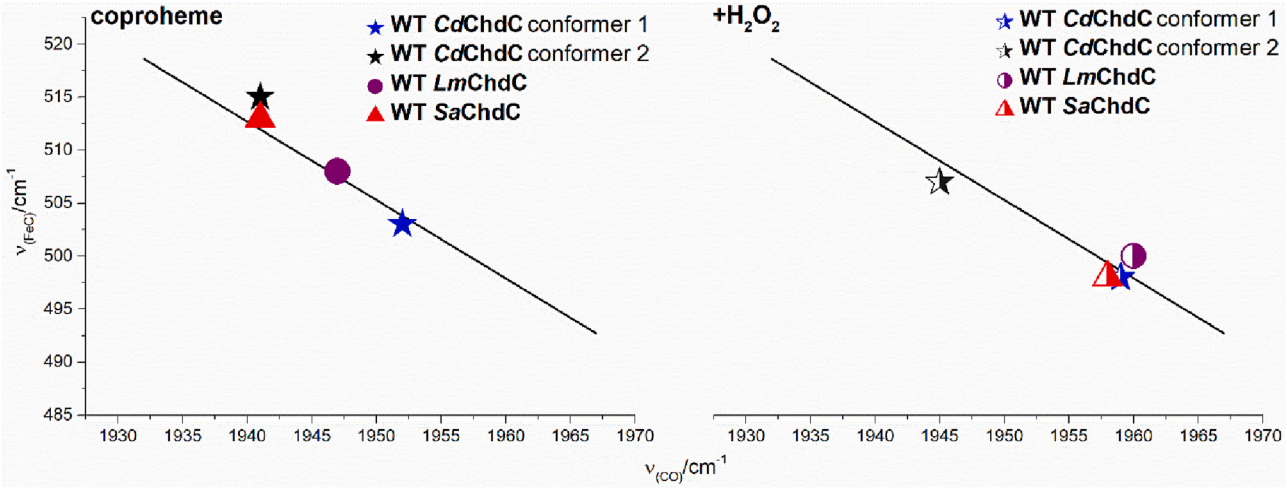

Fig. 11. Back-bonding correlation of the $\nu_{(FeC)}$ and $\nu_{(CO)}$ stretching wavenumbers of the CO adducts of actinobacterial *Cd*ChdC complexed with coproheme complexes before (left) and after (right) hydrogen peroxide titration. The firmicute *Lm*ChdC [56] and *Sa*ChdC [15] complexed with coproheme (left) and heme *b* (right) are also shown. The line has been obtained according to Ref. [31].

90° rotation of the porphyrin ring inside the heme cavity, the role of the distal H118 changes from the stabilization of the incoming ligands to heme *b* binding and subsequent heme *b* release. In fact, mutation of the distal His118 residue with apolar residues alters the capability of the porphyrin ring to bind inside the pocket. The encumbered hydrophobic Phe (H118F) completely prevents the heme *b* insertion, while with the small Ala residue (H118A), the discrimination of the hemin orientation is lost, and mainly a reversed heme is inserted in the active site. The CO data of the reversed heme complex confirm the high flexibility of the active site, not only on the proximal side, as previously reported, but also on the distal side, being the CO binding different from the canonical form.

The effect of the simultaneous rupture of the H-bond interactions with both p_2 and p_4 of the conserved Arg139, typical of actinobacterial ChdCs, alters the architecture of the distal cavity, and the CO binds the heme iron in an open cavity. Similarly, conversion to heme *d*-CO species upon addition of an excess of hydrogen peroxide strongly modifies the distal cavity structure leaving the FeCO unit in a nonpolar environment, consistent with the distal His side chain swung out of the heme pocket.

In conclusion, on the basis of the previous data and on the CO binding properties, we suggest that the overall increased flexibility of the protein cavity in actinobacterial *Cd*ChdC with respect to representatives from Firmicutes might correlate with its higher reactivity toward hydrogen peroxide.

CRediT authorship contribution statement

Federico Sebastiani: Conceptualization, Data curation, Formal analysis, Investigation, Methodology, Supervision, Validation, Visualization, Writing – original draft, Writing – review & editing. **Andrea Dali:** Data curation, Formal analysis, Investigation, Methodology, Visualization, Writing – review & editing. **Diego Javier Alonso de Armiño:** Data curation, Formal analysis, Investigation, Methodology, Visualization, Writing – original draft, Writing – review & editing. **Lorenzo Campagni:** Data curation, Formal analysis, Investigation, Writing – review & editing. **Gaurav Patil:** Data curation, Methodology, Writing – review & editing. **Maurizio Becucci:** Data curation, Methodology, Supervision, Validation, Writing – original draft, Writing – review & editing. **Stefan Hofbauer:** Data curation, Funding acquisition, Supervision, Validation, Writing – review & editing. **Dario A. Estrin:** Conceptualization. **Giulietta Smulevich:** Conceptualization, Data curation, Funding acquisition, Project administration, Supervision, Validation, Writing – original draft, Writing – review & editing.

Declaration of Competing Interest

The authors declare that they have no known competing financial interests or personal relationships that could have appeared to influence the work reported in this paper.

Data availability

Data will be made available on request.

Acknowledgments

This project was supported by EQ-BOKU VIBT GmbH and the BOKU Core Facility Biomolecular & Cellular Analysis. This project was financed by the Austrian Science Fund, FWF, projects P34934, W1224 (S.H.) and Fondazione Cassa Risparmio di Firenze, grant 2020.1397 (G. S.). A.D. is the recipient of a PhD fellowship funded by Italian Ministry of Education, University and Research "Progetto Dipartimenti di Eccellenza 2018–2022" allocated to the Department of Chemistry "Ugo. Schiff" (DICUS).

Appendix A. Supplementary data

Supplementary data to this article can be found online at https://doi.org/10.1016/j.jinorgbio.2023.112243.

References

[1] J.E. Choby, E.P. Skaar, J. Mol. Biol. 428 (2016) 3408–3428.
[2] R.K. Donegan, Y.B. Fu, J. Copeland, S. Idga, G. Brown, O.F. Hale, A. Mitra, H. Yang, H.A. Dailey, M. Niederweis, P. Jain, A.R. Reddi, Microbiol. Spectr. 10 (2022) e03604–e03622.
[3] R.K. Donegan, Biol. Chem. 403 (2022) 1017–1029.
[4] H.A. Dailey, S. Gerdes, T.A. Dailey, J.S. Burch, J.D. Phillips, P Natl. Acad. Sci. U.S. A. 112 (2015) 2210–2215.
[5] H.A. Dailey, T.A. Dailey, S. Gerdes, D. Jahn, M. Jahn, M.R. O'Brian, M.J. Warren, Microbiol. Mol. Biol. R 81 (2017).
[6] G. Layer, Bba-Mol. Cell Res. 1868 (2021).
[7] J.Z. Beas, M.A.M. Videira, L.M. Saraiva, Coord. Chem. Rev. 452 (2022).
[8] S.A. Lobo, A. Scott, M.A. Videira, D. Winpenny, M. Gardner, M.J. Palmer, S. Schroeder, A.D. Lawrence, T. Parkinson, M.J. Warren, L.M. Saraiva, Mol. Microbiol. 97 (2015) 472–487.
[9] Y. Zhang, J.K. Wang, C. Yuan, W. Liu, H.W. Tan, X.C. Li, G.J. Chen, Phys. Chem. Chem. Phys. 22 (2020) 16117–16124.
[10] H. Michlits, B. Lier, V. Pfanzagl, K. Djinovic-Carugo, P.G. Furtmuller, C. Oostenbrink, C. Obinger, S. Hofbauer, ACS Catal. 10 (2020) 5405–5418.
[11] S. Hofbauer, V. Pfanzagl, H. Michlits, D. Schmidt, C. Obinger, P.G. Furtmuller, Bba-Proteins Proteom. 1869 (2021).
[12] B.R. Streit, A.I. Celis, G.C. Moraski, K.A. Shisler, E.M. Shepard, K.R. Rodgers, G. S. Lukat-Rodgers, J.L. DuBois, J. Biol. Chem. 293 (2018) 3989–3999.
[13] F. Sebastiani, H. Michlits, B. Lier, M. Becucci, P.G. Furtmuller, C. Oostenbrink, C. Obinger, S. Hofbauer, G. Smulevich, Biophys. J. 120 (2021) 3600–3614.
[14] L. Milazzo, T. Gabler, D. Puhringer, Z. Jandova, D. Maresch, H. Michlits, V. Pfanzagl, K. Djinovic-Carugo, C. Oostenbrink, P.G. Furtmuller, C. Obinger, G. Smulevich, S. Hofbauer, ACS Catal. 9 (2019) 6766–6782.
[15] A.I. Celis, G.H. Gauss, B.R. Streit, K. Shisler, G.C. Moraski, K.R. Rodgers, G. S. Lukat-Rodgers, J.W. Peters, J.L. DuBois, J. Am. Chem. Soc. 139 (2017) 1900–1911.
[16] W. Liu, Y.J. Pang, Y.T. Song, X.C. Li, H.W. Tan, G.J. Chen, Int. J. Mol. Sci. 23 (2022).
[17] F. Sebastiani, R. Risorti, C. Niccoli, H. Michlits, M. Becucci, S. Hofbauer, G. Smulevich, J. Inorg. Biochem. 229 (2022).
[18] F. Sebastiani, C. Baroni, G. Patil, A. Dali, M. Becucci, S. Hofbauer, G. Smulevich, Biomolecules 13 (2023).
[19] V. Pfanzagl, L. Holcik, D. Maresch, G. Gorgone, H. Michlits, P.G. Furtmuller, S. Hofbauer, Arch. Biochem. Biophys. 640 (2018) 27–36.
[20] R. Timkovich, M.S. Cork, R.B. Gennis, P.Y. Johnson, J. Am. Chem. Soc. 107 (1985) 6069–6075.
[21] K. Sugiyama, R.J. Highet, A. Woods, R.J. Cotter, Y. Osawa, P Natl. Acad. Sci. U.S.A. 94 (1997) 796–801.
[22] L.A. Andersson, T.M. Loehr, C.K. Chang, A.G. Mauk, J. Am. Chem. Soc. 107 (1985) 182–191.
[23] F. Sebastiani, C. Niccoli, H. Michlits, R. Risorti, M. Becucci, S. Hofbauer, G. Smulevich, J. Raman Spectrosc. 53 (2022) 890–901.
[24] S. Hofbauer, B.D. Howes, N. Flego, K.F. Pirker, I. Schaffner, G. Mlynek, K. Djinovic-Carugo, P.G. Furtmuller, G. Smulevich, C. Obinger, Biosci. Rep. 36 (2016).
[25] S. Hofbauer, A. Hagmuller, I. Schaffner, G. Mlynek, M. Krutzler, G. Stadlmayr, K. F. Pirker, C. Obinger, H. Daims, K. Djinoyic-Carugo, P.G. Furtmuller, Arch. Biochem. Biophys. 574 (2015) 36–48.
[26] S. Hofbauer, G. Mlynek, L. Milazzo, D. Puhringer, D. Maresch, I. Schaffner, P. G. Furtmuller, G. Smulevich, K. Djinovic-Carugo, C. Obinger, FEBS J. 283 (2016) 4386–4401.
[27] B.R. Streit, A.I. Celis, K. Shisler, K.R. Rodgers, G.S. Lukat-Rodgers, J.L. DuBois, Biochemistry-Us 56 (2017) 189–201.
[28] B.R. Streit, B. Blanc, G.S. Lukat-Rodgers, K.R. Rodgers, J.L. DuBois, J. Am. Chem. Soc. 132 (2010) 5711–5724.
[29] A.I. Celis, B.R. Streit, G.C. Moraski, R. Kant, T.D. Lash, G.S. Lukat-Rodgers, K. R. Rodgers, J.L. DuBois, Biochemistry-Us 54 (2015) 4022–4032.
[30] G.N. Phillips, M.L. Teodoro, T.S. Li, B. Smith, J.S. Olson, J. Phys. Chem. B 103 (1999) 8817–8829.
[31] T.G. Spiro, I.H. Wasbotten, J. Inorg. Biochem. 99 (2005) 34–44.
[32] H. Michlits, N. Valente, G. Mlynek, S. Hofbauer, Front Bioeng, Biotech 9 (2022).
[33] L. Capece, D.A. Estrin, M.A. Marti, Biochemistry-Us 47 (2008) 9416–9427.
[34] L. Capece, L. Boechi, L.L. Perissinotti, P. Arroyo-Manez, D.E. Bikiel, G. Smulevich, M.A. Marti, D.A. Estrin, Bba-Proteins Proteom. 1834 (2013) 1722–1738.
[35] A.D. Nadra, M.A. Marti, A. Pesce, M. Bolognesi, D.A. Estrin, Proteins 71 (2008) 695–705.
[36] R. Salomon-Ferrer, D.A. Case, R.C. Walker, Wires Comput. Mol. Sci. 3 (2013) 198–210.
[37] H.J.C. Berendsen, J.P.M. Postma, W.F. Van Gunsteren, A. Dinola, J.R. Haak, The Journal of Chemical Physics 81, American Institute of PhysicsAIP, 1984, pp. 3684–3690.
[38] M.P. Allen, D.J. Tildesley. Computer Simulation of Liquids, Oxford University Press, New York, 1987.
[39] A. Ghosh, D.F. Bocian, J. Phys. Chem.-Us 100 (1996) 6363–6367.

[40] G.B. Ray, X.Y. Li, J.A. Ibers, J.L. Sessler, T.G. Spiro, J. Am. Chem. Soc. 116 (1994) 162–176.
[41] T. Uno, Y. Nishimura, M. Tsuboi, R. Makino, T. Iizuka, Y. Ishimura, J. Biol. Chem. 262 (1987) 4549–4556.
[42] S. Brogioni, A. Feis, M.P. Marzocchi, M. Zederbauer, P.G. Furtmuller, C. Obinger, G. Smulevich, J. Raman Spectrosc. 37 (2006) 263–276.
[43] S.Z. Hu, K.M. Smith, T.G. Spiro, J. Am. Chem. Soc. 118 (1996) 12638–12646.
[44] D. Morikis, P.M. Champion, B.A. Springer, S.G. Sligar, Biochemistry-Us 28 (1989) 4791–4800.
[45] F. Sebastiani, L. Milazzo, C. Exertier, M. Becucci, G. Smulevich, J. Raman Spectrosc. 52 (2021) 2536–2549.
[46] F. Rwere, P.J. Mak, J.R. Kincaid, Biochemistry-Us 47 (2008) 12869–12877.
[47] J. Sun, C.K. Chang, T.M. Loehr, J. Phys. Chem. B 101 (1997) 1476–1483.
[48] T.K. Das, E.K. Wilson, F. Cutruzzola, M. Brunori, D.L. Rousseau, Biochemistry-Us 40 (2001) 10774–10781.
[49] V. Guallar, B. Olsen, J. Inorg. Biochem. 100 (2006) 755–760.
[50] T. Hayashi, K. Harada, K. Sakurai, H. Shimada, S. Hirota, J. Am. Chem. Soc. 131 (2009), 1398-+.
[51] H. Yoshimura, S. Yoshioka, K. Kobayashi, T. Ohta, T. Uchida, M. Kubo, T. Kitagawa, S. Aono, Biochemistry-Us 45 (2006) 8301–8307.
[52] R. Evangelista-Kirkup, G. Smulevich, T.G. Spiro, Biochemistry-Us 25 (1986) 4420–4425.
[53] T.S. Li, M.L. Quillin, G.N. Phillips, J.S. Olson, Biochemistry-Us 33 (1994) 1433–1446.
[54] F. Yang, G.N. Phillips, J. Mol. Biol. 256 (1996) 762–774.
[55] G. Smulevich, M. Paoli, G. DeSanctis, A.R. Mantini, F. Ascoli, M. Coletta, Biochemistry-Us 36 (1997) 640–649.
[56] L. Milazzo, S. Hofbauer, B.D. Howes, T. Gabler, P.G. Furtmuller, C. Obinger, G. Smulevich, Biochemistry-Us 57 (2018) 2044–2057.